Validated physical models and parameters of bulk 3C-SiC aiming for credible Technology Computer Aided Design (TCAD) simulation

Arvanitopoulos A.[1], Lophitis N.[1], Gyftakis K. N.[1], Perkins S.[1] and Antoniou M.[2]

[1] Faculty of Engineering, Environment and Computing, Coventry University, Coventry, UK
[2] Electrical Engineering, University of Cambridge, Cambridge, UK

arvanita@uni.coventry.ac.uk

Abstract. The cubic form of SiC (β- or 3C-) compared to the hexagonal α-SiC polytypes, primarily 4H- and 6H-SiC, has lower growth cost and can be grown heteroepitaxially in large area Silicon (Si) wafers which makes it of special interest. This in conjunction with the recently reported growth of improved quality 3C-SiC, make the development of devices an imminent objective. However, the readiness of models that accurately predict the material characteristics, properties and performance is an imperative requirement for attaining the design and optimization of functional devices. The purpose of this study is to provide and validate a comprehensive set of models alongside with their parameters for bulk 3C-SiC. The validation process revealed that the proposed models are in a very good agreement to experimental data and confidence ranges were identified. This is the first piece of work achieving that for 3C-SiC. Considerably, it constitutes the necessary step for Finite Element Method (FEM) simulations and Technology Computer Aided Design (TCAD).

1. Introduction

Wide bandgap (WBG) semiconductors feature a wider bandgap ($> 2eV$) compared to Silicon (Si). They are of increased interest, because Si technology is reaching its performance limitations especially for power electronic systems [1]. Higher temperature, voltage and frequency operation are among the attributed superior properties the devices can achieve when WBG materials are used. Silicon Carbide (SiC) and Gallium Nitride (GaN) currently stand as the best WBG semiconductor candidates to replace Si [2]. Nonetheless, the SiC process technologies are currently considered more mature [3].

SiC may occur with many different crystal structures, also known as polytypes, with the stacking sequence. Depending on the stacking order of the tetrahedrally bonded Si-C bilayers [4], the silicon and carbon atoms on adjacent bilayer planes is either of cubic or hexagonal nature [5]. The 3C-SiC, also encountered as β-SiC, is the only form of SiC with a cubic crystal structure. The non-cubic polytypes of SiC are referred to as α-SiC. Among the many hexagonal structures, 4H- and 6H- are the most researched ones. The 4H-SiC has been favored as the SiC candidate of choice for high power and high frequency applications because of the highest bandgap energy. The 3C-SiC, however, features specific advantageous properties which also make it highly desired for power devices. The main advantage of the cubic SiC polytype is the lower fabrication cost [6]. In terms of crystal growth, the process is compatible with the Si technology. The cubic SiC polytype can be grown heteroepitaxially on Si wafers and the required growth temperatures are lower than those required when processing 4H-SiC. Moreover,

the 3C-SiC can also be advantageous from a device-level perspective. In particular, a decrement of the defects density at the SiO_2/3C-SiC interface is observed when Metal Oxide Semiconductor (MOS) devices are required [7][8][9]. The latter essentially contributes to increasing the mobility for both carriers' types at higher levels compared to 4H-SiC. Further, the lower bandgap of β-SiC leads to achieving channel inversion at reduced electric field levels in the case of Metal Oxide Semiconductor Field Effect Transistors (MOSFETs) [10]. Finally, it has been demonstrated that the stacking faults in the 3C-SiC material do not affect its operation [11], as evidenced in the case of 4H-SiC, due to propagation phenomena [12]. In addition, the cubic structure imparts higher electrical propertied isotropy [6].

Almost all power device types have been demonstrated with the 3C-SiC compound. Schottky Barrier Diodes (SBDs) [13][14], PiN devices [15][16] and MOSFETs [17][18]. These works however, conclude that the observed performance is far below from what expected for devices made of SiC crystals. Taking into account that the performance is dominated by the material quality, cubic SiC polytype is not yet described as a matured technology and is open to advancements [19]. Accurate modelling of the 3C-SiC material properties for Technology Computer Aided Design (TCAD) simulations would be a major step forward for this polytype. This is because TCAD assists power semiconductor device development including the achievement of optimized performance [20] and high reliability [21]. Published works denote the interest of modelling 3C-SiC power devices [22] and simulating with Monte Carlo method [23][24]. Initial efforts to describe the cubic-polytype of SiC in TCAD tools are present [25] as well with simulations in device level [26][27][28]. Nonetheless, the physical models for 3C-SiC are immature and significant research is still required [27]. Moreover, to the best of the authors' knowledge, no reports on a validated complete parametrization of the cubic SiC polytype for accurate FEM analysis have been presented.

The contribution of this paper is to provide and validate the physics models and the corresponding material parameter sets of the bulk β-SiC polytype. The importance of this work is further enhanced by recent advancements in grown 3C-SiC crystal quality. Indicatively, a 380nm thick p-type single crystalline 3C-SiC has been grown on a p-type Si (100) substrate [29]. Likewise, a good quality of 1μm 3C-SiC hetero-epitaxially grown on Si has been reported [30]. It is therefore, not unreasonable to argue that 3C-SiC may be an excellent candidate for power devices that can soon become a commercial reality, featuring thin layers of material. Consequently, the existence of an accurate and valid TCAD material model will be of great value for the research on this polytype on such power devices to be lifted up.

The remaining sections of this article are organized as follows. The section 2 is separated into subsections, each one dealing with a parameter set of the 3C-SiC polytype under discussion. Leading to specific material coefficient values fine-tuning, the validation processes for the physical models involved are presented, utilizing MATLAB. Finally, the conclusions of this work are illustrated in section 3.

2. The physical model of 3C-SiC

In this section the various parameters inherent to the material are identified and modelled. To accurately predict the performance of devices that use 3C-SiC as the preferred material, it is necessary to accurately model the properties, the electrical characteristics of the material and carrier transport and recombination phenomena. It is also important to model how those properties, characteristics and phenomena change, for example as a function of temperature, doping concentration and electric field. Each model and parameter set described in this work constitutes an information "brick" of the material entity in TCAD tools. The information that each of these "bricks" carries, regarding a specific physical property of the 3C-SiC, is validated separately with comparisons to experimental data available in literature. Putting these bricks together allows Finite Element Method (FEM) and TCAD simulations to be carried out and to analyze the behavior of devices based on the cubic SiC polytype.

2.1. Bandgap parameters for 3C-SiC

The desired properties demonstrated by WBG semiconductors are mainly attributed to their bandgap characteristics. Nonetheless, the effective bandgap results from the temperature dependent bandgap value reduced by the term representing the bandgap narrowing phenomenon, E_{bgn}, as shown in (1).

$$E_{g,eff}(T) = E_g(T) - E_{bgn} \quad (1)$$

The band gap dependence on the lattice temperature is described in (2), where $E_g(0)$ is the band gap energy at 0 Kelvin and α, β are material parameters [31]. 3C-SiC is an indirect semiconductor material and the energy gap is defined as the minimum distance of maximum valence band (Γ15) to minimum of the conduction band (X1C) resulting in $E_g(0) = \Gamma_{15}^u - X_1^c = 2.39eV$. Further, the parameters α and β are determined in this work to fit available 3C-SiC measurement data as shown in Fig. 1.

$$E_g(T) = E_g(0) - \alpha T^2/(T+\beta) \quad (2)$$

The 3C-SiC bandgap dependence on temperature, following the (2), was initially described in [32]. In this work, further fine-tuning of the parameters α, β, according to experimental data in [33], determine their values as presented in Table I. As shown in Fig. 1, very good matching has been achieved.

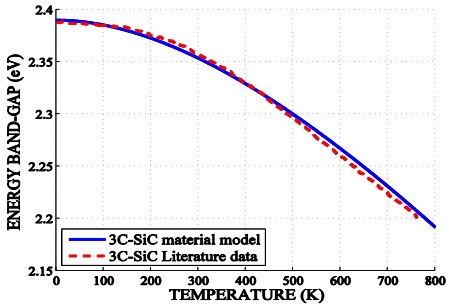

Fig. 1: The 3C-SiC bandgap dependence on temperature as described in (2) utilizing the material parameters determined in this work. Literature data for comparison are from [33].

Table I: *3C-SiC parameter set related to Bandgap.*

Parameters Description	***3C-SiC***
$E_g(0)$ [eV]	*2.39*
α [eV/K]	*$0.66x10^{-3}$*
β [K]	*1335*

Bandgap narrowing refers to the case where doping concentration causes displacements in the energy scale of the 3C-SiC Γ_{15}^u and X_1^c bands. According to [34], the behavior of power devices that contain layers with different doping profiles may be affected, leading to band-edge displacements. These displacements representing potential barriers, influence carrier transport phenomena in the device and their interactions. The main difference of the various bandgap models available is how they handle bandgap narrowing. In equation (3), the term ΔE_g^0 is determined by the particular bandgap narrowing model used, and ΔE_g^{Fermi} is an optional correction to account for carrier statistics. In this work the Maxwell–Boltzmann statistics are considered when investigating the dynamics of a collection of carriers. For power devices that their size is relatively large, compared to the de Broglie wavelength of electrons this correction term is negligible.

$$E_{bgn} = \Delta E_g^0 + \Delta E_g^{Fermi} \quad (3)$$

Furthermore, Lindefelt [34] proposed a model for the band-edge displacements of n-type 3C-SiC material, valid for majority carriers concentrations typically above 10^{18}cm^{-3}. This model essentially constitutes an extension of the Jain-Roulston (J-R) theory [35] implemented in TCAD tools to describe the doping dependence on bandgap narrowing (ΔE_g^0) as presented in (4). Thus, the resulting narrowing of the band gap is due to conduction and valence band displacements and is defined in such a way to be a positive quantity. The conduction band displacements (E_{bgn}^{cond}) description due to the high levels of doping are shown in (5a) for the case of an n-type 3C-SiC material region, and in (5b) for the case of a p-type region. Regarding the valence band, the formulas presented in (6a) and (6b) describe the displacements (E_{bgn}^{val}) for n-type and p-type 3C-SiC material respectively. In these equations, the terms $A_{n,p}$, $B_{n,p}$, $C_{n,p}$, and $D_{n,p}$ are material dependent coefficients, which depict the energy distance between the valence band and conduction band shifts in eV.

$$\Delta E_g^0 = -E_{bgn}^{cond} + E_{bgn}^{val} \quad (4)$$

$$E_{bgn}^{cond} = \begin{cases} A_n \cdot N_{tot}^{1/3} + C_n \cdot N_{tot}^{1/2}, & N_{D,0} > N_{A,0} \quad (5a) \\ B_p \cdot N_{tot}^{1/4} + D_p \cdot N_{tot}^{1/2}, & otherwise \quad (5b) \end{cases}$$

$$E_{bgn}^{val} = \begin{cases} B_n \cdot N_{tot}^{1/4} + D_n \cdot N_{tot}^{1/2}, & N_{D,0} > N_{A,0} \quad (6a) \\ A_p \cdot N_{tot}^{1/3} + C_p \cdot N_{tot}^{1/2}, & otherwise \quad (6b) \end{cases}$$

By following the work in [34] the values of the parameters in the original J-R model can be adjusted, to those presented in Table II in order to get the best matching possible to the available corresponding data for 3C-SiC. These coefficient values are calculated in such a way that for low doping concentration, that is below 10^{18}cm^{-3}, the band edge displacements of the material will be negligible. In Fig. 2 and Fig. 3 a comparison of the J-R model utilizing the parameter values of Table II and the relative data in literature [36] is illustrated. It can be seen that the band gap narrowing in n-doped 3C-SiC semiconductor is larger than in p-doped for the same concentrations of dopants. This is in excellent agreement to the findings in [34].

Table II: *3C-SiC band gap narrowing doping dependence.*

Lindefelt model coefficients	***3C-SiC semiconductor material***	
	n-type	***p-type***
$A_{n,p}$ [eV·cm]	*-1.48x10^{-8}*	*1.3x10^{-8}*
$B_{n,p}$ [eV·cm$^{3/4}$]	*9.0x10^{-7}*	*-4.8x10^{-7}*
$C_{n,p}$ [eV·cm$^{3/2}$]	*-3.06x10^{-12}*	*1.43x10^{-12}*
$D_{n,p}$ [eV·cm$^{3/2}$]	*6.85x10^{-12}*	*-6.41x10^{-13}*

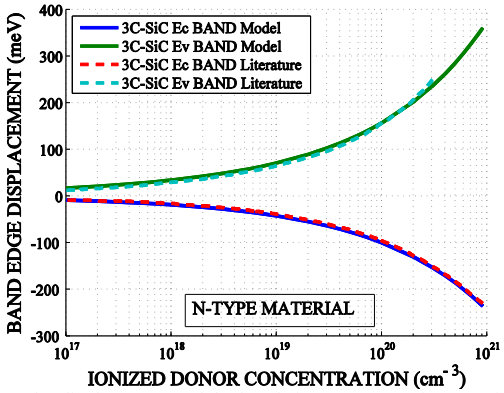

Fig. 2: The displacements of the bands in n-type 3C-SiC material due to doping, utilizing the parameters fine-tuned in this work. Literature data are sourced from [36].

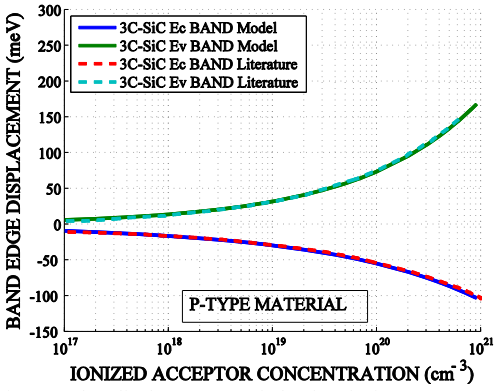

Fig. 3: The displacements of the bands in p-type 3C-SiC material due to doping, utilizing the parameters fine-tuned in this work.

The electron affinity (χ) describes the separation between the conduction band (E_C) and the vacuum level (E_0). Particularly, the electron affinity is necessary to construct informative band diagrams and data in literature is rather contradictory [37]. In the J-R model the χ depends on both the temperature and the doping especially for high concentrations. The model expression is presented in (7). The quantity E_{bgn}^{cond} indirectly reflects the doping dependence of the electron affinity. Furthermore, the coefficients α_2 and β_2 are set to be equal to zero. This specific considered model allows for the usage of these extra fitting parameters to fine tune the χ dependence on temperature without affecting the corresponding bandgap dependence. The discussed parameter values for the J-R affinity model are presented in Table III.

$$\chi(T, N_{A,0}, N_{D,0}) = \chi_0 + \frac{(\alpha + \alpha_2)T^2}{2(T + \beta + \beta_2)} + E_{bgn}^{cond} \quad (7)$$

Table III: *3C-SiC parameter set related to Affinity.*

Parameters Description	***3C-SiC***
Electron affinity [eV]	*3.83*
α_2 [eV/K]	*0*
β_2 [K]	*0*

In addition, from [32] [38], the static dielectric constant of the cubic SiC is defined as $\varepsilon_0^{3C} = 9.72$.

2.2. Density of states (DoS) in the conduction and valence bands

The carrier effective masses and densities of states quantities are directly related to each other. According to the literature, computing the effective carrier mass as a function of temperature-dependent DoS is an option that best suits the parameters for 3C-SiC available in the literature. Taking into account the work in [39] and [40], the models described by (8a) and (8b) can be deployed.

$$N_C = 2M\left(\frac{2\pi k}{h^2}\right)^{\frac{3}{2}} (m_c/m_0)^{\frac{3}{2}}\ T^{\frac{3}{2}} \tag{8a}$$

$$N_V = 2\left(\frac{2\pi k}{h^2}\right)^{\frac{3}{2}} (m_v/m_0)^{\frac{3}{2}}\ T^{\frac{3}{2}} \tag{8b}$$

$$N_C = 2.99 \times 10^{15} \times T^{\frac{3}{2}}\ (cm^{-3}) \tag{9a}$$

$$N_V = 2.24 \times 10^{15} \times T^{\frac{3}{2}}\ (cm^{-3}) \tag{9b}$$

$$N_{C,V}(T) = N_{C,V}300 \times \left(\frac{T}{300}\right)^{\frac{3}{2}} \tag{10}$$

Table IV: *3C-SiC temperature dependent Density of States.*

Parameters Description	***3C-SiC***
N_C (300K) [cm^{-3}]	*1.5536x10^{19}*
N_V (300K) [cm^{-3}]	*1.1639x10^{19}*

In the above equations, $M = 3$ represents the number of equivalent valleys in the conduction band, $m_c = 0.35m_0$ is the effective mass of the DoS in one valley of conduction band and $m_v = 0.6m_0$ is the effective mass of density of state in the one valley of valence band, all considered for $T = 300$K [36]. Substituting these values in the model for the DoS in 3C-SiC the simplified expressions (9) are derived. By applying the latter formulas, the parameter values required to model the DoS dependence on temperature are determined and summarized in Table IV. This dependence is described in (10) and illustrated in Fig. 4.

Additionally, the intrinsic carrier concentration (n_i) is directly proportional to N_C and N_V, which are the conduction and valence band DoS respectively, as expressed in (11). The n_i is the result of the thermal expansion of the lattice and electron-phonon coupling. Thus, it features an exponential dependence upon temperature, as well as the band gap value. Essentially, it is determined by the thermal generation of electron-hole pairs across the energy bandgap [40] [41]. Therefore, the intrinsic carrier concentration is indicative for the ability of a semiconductor material to maintain its characteristics at elevated temperatures. The Table V presents the n_i values calculated for $T = 200$K and $T = 300$K taking into account the DoS temperature dependence. In Fig. 5, the 3C-SiC intrinsic carrier concentration, taking into account both the DoS and bandgap dependencies on temperature as described in subsection 2.1, is presented and compared to literature values. As seen, the model proposed in this paper has matched the measurements [42] reasonably well for the range of values $200\text{K} < T < 500\text{K}$.

$$n_i = \sqrt{N_C N_V}\, exp\left(-E_g/2kT\right) \tag{11}$$

Table V: *3C-SiC Intrinsic carrier concentration as a function of temperature dependent Density of States.*

Parameters Description	***3C-SiC***
Intrinsic carrier concentration n_i [cm^{-3}] *T=200*K *(with $E_g = E_g(T)$)*	*9.888x10^{-11}*
Intrinsic carrier concentration n_i [cm^{-3}] *T=300*K *(with $E_g(T)$)*	*2.285x10^{-1}*

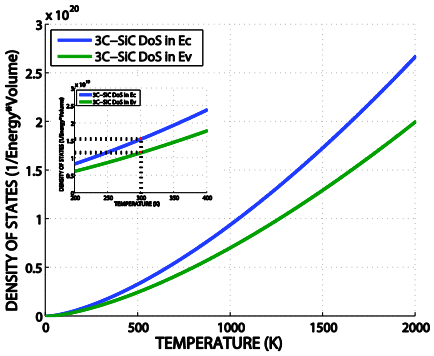

Fig. 4: The Density of States in both conduction and valence band plotted against temperature for the 3C-SiC. The inset plot focuses at the area of the graph for temperature values close to 300K.

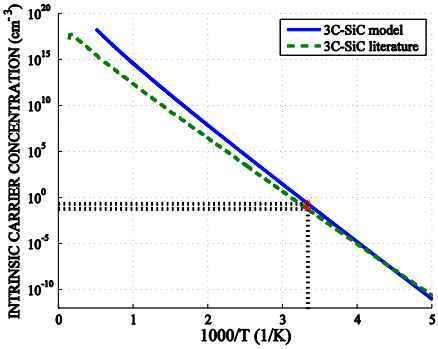

Fig. 5: Assuming low doping or unintentional doping levels ($5x10^{15}\text{cm}^{-3}$) the intrinsic carrier concentration against temperature is compared with n_i measurements [42]. Thus, the resulting bandgap narrowing is negligible in this case.

2.3. Carrier Mobility in 3C-SiC

2.3.1. Low – field Mobility

Doping Dependence

The main building blocks of power devices are the junctions formed between doped regions of the material. Consequently, the accurate modeling of the doping effect on the carrier mobility is important. One of the most frequently used models to describe the doping dependence of carriers mobility in the semiconductor is the Arora model [43]. The Caughey – Thomas (C-T) expression [44] approximates this model for low applied electric field conditions. The C-T formula is shown in (12) where, N is the total doping concentration, μ_{max} is the mobility of undoped or unintentionally doped samples, μ_{min} is the mobility in highly doped material, N_{ref} is the doping concentration at which the mobility is halfway between its minimum and maximum value and α is a measure of how quickly the mobility changes in this range. However, in [45] it is stated that this model fails for the case of 3C-SiC as there does not appear to be a definite value for μ_{min}. Thus, an alternative model for electron mobility that behaves like the C-T expression for low doping and like Powel's [46] for high doping is proposed.

In this work, experimental data available in [45] is utilized and various values for the minimum mobility are investigated with the C-T expression in MATLAB. For the range of doping concentrations from $1 \times 10^{14}\text{cm}^{-3}$ to $1 \times 10^{22}\text{cm}^{-3}$ a minimum mobility value of $40\text{cm}^2/\text{Vs}$ is used. The values for the holes parameters $\mu_{max}^{h^+}$ and $\mu_{min}^{h^+}$ suggested from measurements in [47], [36] differ from the values adopted in this work. After curve fitting to the available data [36] [48], slightly greater values of the maximum holes mobility are considered.

The low field parameters for the 3C-SiC electron mobility, supplemented with values for holes, are summarized and presented in Table VI for a temperature of $T = 300\text{K}$. The modelled dependence of the electrons' mobility in 3C-SiC for the doping concentration, is presented in Fig. 6. In comparison, experimental data from [45] and [49] have also been plotted. The parameters determined for the C-T model in this work describe accurately enough the 3C-SiC mobility dependence on doping, especially for the range of values $5 \times 10^{15}\text{cm}^{-3} < N_{D,A} < 1 \times 10^{20}\text{cm}^{-3}$. For the holes case, the high discrepancy of the alternative Powel/C-T formula, in Fig. 7, should be noticed. This model [45] was developed initially for 3C-SiC electrons' mobility and therefore, it fails to accurately describe the corresponding holes behavior.

It also should be noted that, recent works, relate the mobility of the grown 3C-SiC crystal directly to its thickness. The thicker the material the better its mobility characteristics [50]. This fact may imply the dependence of this physical entity on the material defects. A thick enough grown crystal ($> 30\mu\text{m}$) reduces the effect of shallow centers and traps formed at the 3C-SiC interface with the substrate wafer due to mismatches [51] [52]. Thus, the dominant mechanism to determine the carrier mobility is

scattering from interfaces and impurities and not the intrinsic band structure due to carrier interaction with the lattice [53]. For accurate device modeling, this variability should be taken into consideration. The device can be discretized in regions of different μ_{min} values for the bulk model presented in this work.

$$\mu_0 = \mu_{min} + (\mu_{max} - \mu_{min})/\left(1 + \left(N/N_{ref}\right)^{\alpha}\right) \tag{12}$$

Table VI: *3C-SiC parameters for low Field mobility and coefficients used to express doping dependence.*

Parameter	***3C-SiC***	
	electrons	***holes***
μ_{max} [cm^2/Vs]	*650*	*70*
μ_{min} [cm^2/Vs]	*40*	*15*
N_{ref} [cm^{-3}]	*1.5x10^{17}*	*5x10^{19}*
α	*0.8*	*0.3*

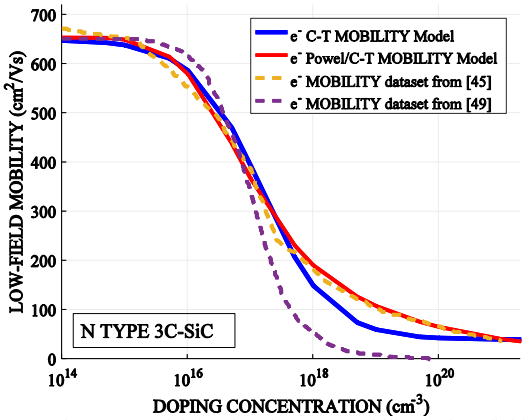

Fig. 6: The C-T model for the electrons mobility in low fields for various values of doping densities is utilized with the coefficients determined in this work. The Powel/C-T model [45] is also plotted for comparison.

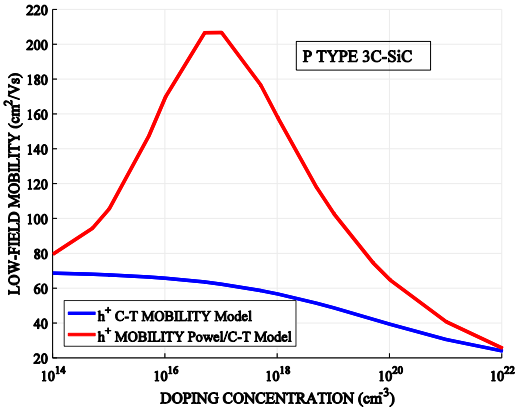

Fig. 7: The Powel/C-T model [45] is not designed to fit the holes mobility behavior. The discrepancy is noticeable in this plot. The C-T model performs closer to what expected since no relative measurements are available for the 3C-SiC.

Temperature Dependence

When aiming to accurately capture the temperature dependency of mobility, a more complex approach should be considered. This is because many other parameters may also be affected. Assuming an n-type material, the Fermi level measured from the conduction band changes with temperature and so do all the parameters involved in the mobility description. Exactly the same behavior is expected for a p-type material, in the difference of a changeable distance to the valence band this time. Small variations of the relative position of the Fermi level imply a changing doping concentration value [50], according to (13). The temperature dependence for the low-field mobility parameters is described by (14), where Par is the parameter of interest from Table VI and Par_0 is the value of the parameter at 300 Kelvin. The 3C-SiC mobility experimental dataset in [50] is used. The equation in (14) was found to give a good match with the experimental dataset available when the values of Table VII are utilized, in particular, $\gamma_{min}^{e^-} = \gamma_{min}^{h^+} = -0.5$ for the parameter μ_{min}. In addition, the temperature coefficient for the parameter $\mu_{max}^{e^-}$ used was $\gamma_{max}^{e^-} = -0.3$. It was found that these parameters strongly affect the performance of the C-T model for the high field mobility (presented in the next subsection). Thus, no further fine-tuning was attempted. Indeed, the matching with the experimental results is close for the range of temperatures that are of typical interest. For the holes mobility model, the value of $\gamma_{max}^{h^+} = -2.5$ resulted the best possible fit to experimental data of [36]. The determined exponential coefficient values, to describe the temperature dependence of the low field mobility in bulk 3C-SiC material, are summarized in Table VII.

$$n = N_C exp(-(E_C - E_F)/kT) \tag{13a}$$
$$p = N_V exp(-(E_F - E_V)/kT) \tag{13b}$$

$$Par = Par_0 \times (T/300K)^{\gamma} \quad (14)$$

Table VII: *3C-SiC parameters for low Field mobility and coefficients used to express temperature dependence.*

Parameter	*3C-SiC*		*Corresponding parameter from Table VI*
	electrons	*holes*	
γ_{max}	*-0.3*	*-2.5*	μ_{max} [cm^2/Vs]
γ_{min}	*-0.5*	*-0.5*	μ_{min} [cm^2/Vs]
γ_{Nref}	*2*	*0*	N_{ref} [cm^{-3}]
γ_{α}	*0*	*0*	α

The results presented in Fig. 8 imply that the C-T model in the case of 3C-SiC is consistent to the experimentally measured Hall mobility with temperature plotted in [36]. Considering a temperature range of $250\text{K} < T < 700\text{K}$ the deviation of the model from the expected mobility values is small. It can be mentioned that the C-T model works much better for the positive moving carriers as well, especially when the focus is on the range of 300K up to 600K, as shown in Fig. 9. Power devices usually aim to operate within this range of temperature values [54]. We therefore conclude that, the overall behavior of the C-T model for both electrons and holes describes better the mobility dependence on temperature. Consequently, the C-T model parameters determined in this subsection are suitable for investigating 3C-SiC power devices in a wide operational temperature range.

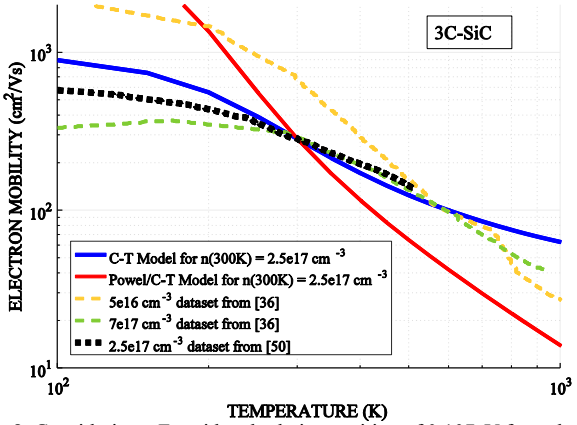

Fig. 8: Considering a Fermi level relative position of 0.107eV from the conduction band, the resulting doping concentration, utilizing (13a), is $2.5x10^{17}\text{cm}^{-3}$. The C-T model performance for a range of temperature values is very close to the corresponding literature electron mobility data [50]. For comparison, the Powel/C-T model is also plotted for the same conditions.

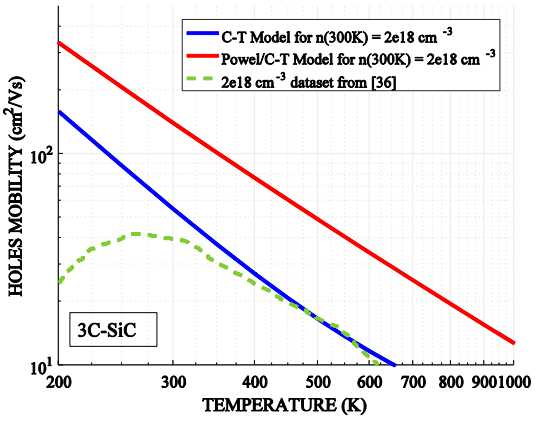

Fig. 9: To compare the performance of the C-T model to available literature data for 3C-SiC holes mobility against temperature, a Fermi level relative position of 0.0455eV from the valence band is considered. Utilizing (13b) this results a doping of $2x10^{18}\text{cm}^{-3}$. Noticeable, the C-T model makes a good fit in a specific range of temperature values.

2.3.2. High – field Mobility

The presence of high electric field strongly affects the carriers' mobility. The Canali model [55] can be used to specify how carriers' mobility varies with the applied electric field, while its expression is shown in (15). It utilizes the formula for the low field mobility (μ_{low}) including additional parameters, the β and v_{sat}, whereas E is the electric field strength. Consequently, following the (14), the values of parameters β_0 and γ_{β} should be determined. Whenever used, the zero subscript denotes a temperature independent coefficient. This is achieved by matching the behavior of our model to the results of the model proposed in [45]. The saturated carriers' velocity temperature exponential $v_{sat,exp}$ and its value is determined indirectly by using (16). According to [56], the nonlinear dependence of the electron drift velocity on electric field for SiC polytypes is expressed in (17). Utilizing the parameters for mobility from Table VI, the value of $v_{sat,0} = 2.5 \times 10^7\,\text{cm/s}$ [57] and equation (17), the parameter $v_{sat,exp}$ from (16) can be fitted to the data presented in [58]. The parameters for the high field mobility dependence are summarized in Table VIII.

Shifting from the low to high field conditions, the mobility and velocity terms essentially become inseparable directly affecting each other as described in (15). Thus, after evaluating the determined

parameter values in this subsection, the Fig. 10 is plotted. It illustrates the mobility evolution for increasing electric field values at specific temperatures. In this, the variation of v_{sat} with the temperature has been taken into account. Further, for the same temperature values, in Fig. 11 and Fig. 12 the velocity versus the applied field is depicted for both electrons and holes carriers in 3C-SiC. As shown, our proposed models achieve good matching for high electric field conditions, especially for values higher than 100kV/cm.

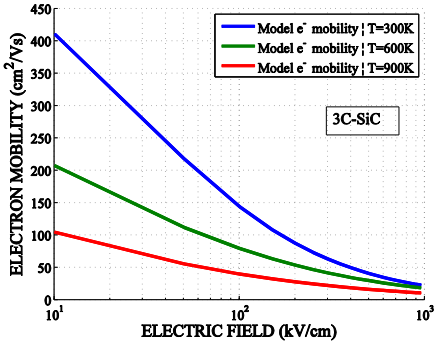

Fig. 10: The 3C-SiC electron mobility is plotted against the applied electric field as described in (15) utilizing the determined parameters from Table V for specific temperature values.

Table VIII: *3C-SiC parameters for high Field mobility and saturation velocity along with coefficients used to express temperature dependence.*

Parameter	***3C-SiC***	
	electrons	***holes***
beta (β_0)	*0.75*	*2.5*
γ_{beta}	*-0.9*	*0*
alpha (α)	*0*	*0*
$v_{sat,0}$ [cm/sec]	$2.5x10^7$	$1.63x10^7$
$v_{sat,exp}$	*-0.65*	*1.55*

$$\mu_0(E) = \frac{(\alpha+1)\mu_{low}}{\alpha + \left[1 + \left(\frac{(\alpha+1)\mu_{low}E}{v_{sat}}\right)^{\beta}\right]^{1/\beta}} \tag{15}$$

$$v_{sat} = v_{sat,0}\left(\frac{300K}{T}\right)^{v_{sat,exp}} \tag{16}$$

$$v = \mu_0(E) \cdot E \tag{17}$$

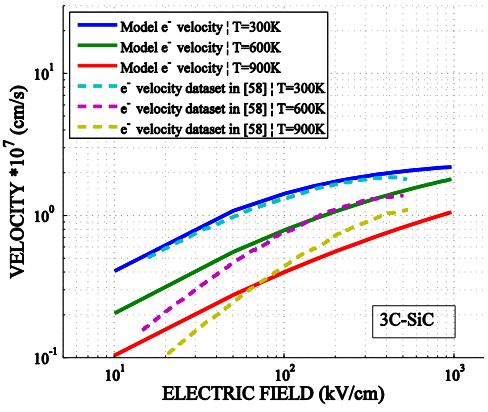

Fig. 11: The electrons velocity for various electric field values, considering a doping density of $5x10^{15}\text{cm}^{-3}$. The parameters determined in this subsection along with the parameters determined for the low-field mobility make a very good match with literature data for temperatures up to 600K.

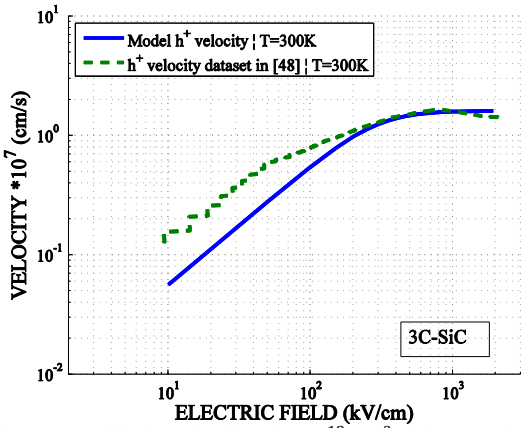

Fig. 12: Considering a density of $1x10^{18}\text{cm}^{-3}$ of dopants, the holes velocity in 3C-SiC match the available literature data for the range of values 200kV/cm < E < 2000kV/cm. Further, towards the upper limit of this range, saturation is observed. This behavior justifies the low-field mobility parameter values determined in 2.3.1 for the C-T model.

2.4. Impact Ionization

The main parameters required for the calculation of the breakdown voltage and the critical electric field, are the ionization coefficients of electron and holes. These are considered constant and material dependent. It is found in [59] that the impact ionization coefficients of bulk 3C-SiC are relatively insensitive to temperature variations in the range of $300\text{K} < T < 500\text{K}$. In TCAD tools, the "van

Overstraeten de Man" model [60] [61] can be used to model the phenomenon of impact ionization. For 3C-SiC, only the ionization coefficients for holes have been determined experimentally. For electrons it is assumed that they are the same [48]. In (18) the dependence on temperature of the impact ionization coefficients for electrons and holes is modelled. The factor γ with the optical phonon energy $\hbar\omega_{op}$ expresses the temperature dependency of the phonon gas against which carriers are accelerated, where $T_0 = 300\text{K}$. Further, in (19) the dependence of these quantities on electric field is described, where E_{ava} is the driving force for impact ionization. The ionization coefficients for both carriers' types at room temperature are summarized in Table IX [62]. In Fig. 13 the impact ionization rate for the holes in 3C-SiC, as modelled in this subsection, is plotted in comparison to the data published in [48]. As illustrated, the model matched the published data very accurately.

$$\gamma = \frac{\tanh\left(\hbar\omega_{op}/2kT_0\right)}{\tanh\left(\hbar\omega_{op}/2kT\right)} \tag{18}$$

$$\alpha(E_{ava}) = \gamma \cdot \alpha \cdot exp(-\gamma b/E_{ava}) \tag{19}$$

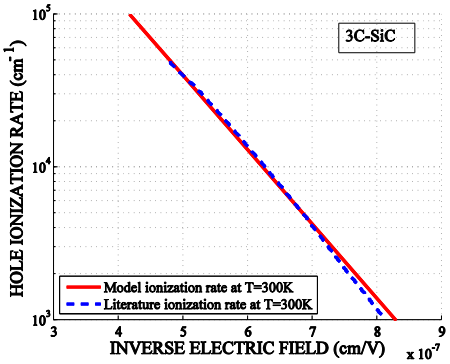

Fig. 13: The hole ionization rate as described by the parameter values in Table IX is in agreement with the available 3C-SiC data in literature. Electrons behavior is assumed to be the same.

Table IX: *3C-SiC impact ionization coefficients.*

Parameters Description	***Parameter Name***	***3C-SiC***
Ionization coefficients for electrons and holes	$a_{n,p}$ [cm^{-1}]	$1.07x10^7$
	$b_{n,p}$ [V/cm]	$1.12x10^7$
Low field range up to this value	E_0 [V/cm]	$4.0x10^5$
Optical phonon energy	$\hbar\omega_{op}$ [eV]	0.120
		0.098

2.5. Incomplete Ionization

The phenomenon of incomplete ionization can be included by modelling the dopant impurities as traps. Depending on the dopant solubility in the semiconductor, the shallow energy level formed is different. This is a first approach of taking into account the existence of shallow defects in the semiconductor model. These levels affect the Fermi-level and describe the available charge carriers needed for conductivity [63]. Following the published works in [64], [65], [66], [67] and [68], the values of Table X present the main impurities in 3C-SiC material due to different specific donor and/or acceptor species.

It is interesting to notice, as illustrated in Fig. 14, that the Boron (B) impurities form deep levels in 3C-SiC, with the activation energy being 0.735eV. This is why it is not considered a good candidate in forming p-type 3C-SiC regions. However, it can be considered for carrier lifetime control engineering [69].

Table X: *3C-SiC impurities / Shallow traps due to doping.*

Impurity	***Species Type***	***Energy Levels* [eV]**
		3C-SiC
Nitrogen (N)	donor [a]	*0.057*
Vanadium (V)	donor [a]	*0.660*
Aluminum (Al)	acceptor [b]	*0.260*
Gallium (Ga)	acceptor [b]	*0.343*
Boron (B)	acceptor [b]	*0.735*

[a] *The formed energy level is considered from the Conduction band (E_C).*

[b] *The formed energy level is considered from the Valence band (E_V).*

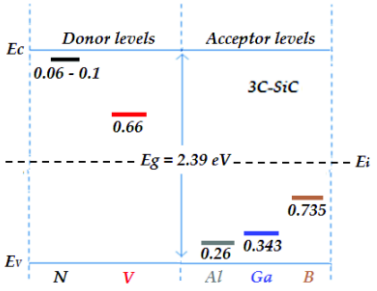

Fig 14: Explicitly trap occupation setting for Nitrogen, Vanadium, Aluminum, Gallium and Boron impurities in cubic SiC [36].

2.6. Schockley-Read-Hall (SRH) Recombination

Generation and recombination mechanisms are very important in power device physics, in particular, for bipolar devices. The SRH expression in (20) describes these recombination processes that are considered dominant for semiconductors with an indirect bandgap [70].

$$R_{net}^{SRH} = \frac{np - n_i^2}{\tau_p(n + n_1) + \tau_n(p + p_1)} \tag{20}$$

$$\tau_{dop} = \tau_{min} + \frac{\tau_{max} - \tau_{min}}{1 + \left(\frac{N_{A,0} + N_{D,0}}{N_{ref}}\right)^{\gamma}} \tag{21}$$

Table XI: *3C-SiC SRH lifetimes parameter set.*

Parameter	***3C-SiC***	
	electrons	***holes***
τ_{min} [sec]	*0*	*0*
τ_{max} [sec]	*2.5x10^{-6}*	*0.5x10^{-6}*
N_{ref}[cm^{-3}]	*1x10^{17}*	*1x10^{17}*
γ	*0.3*	*0.3*

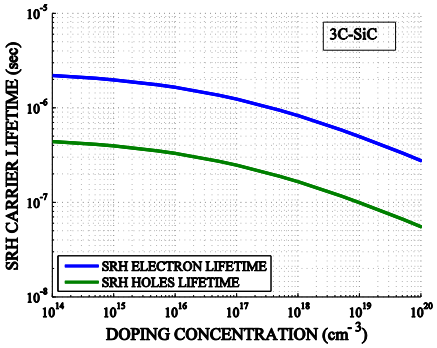

Fig. 15: The SRH carriers' lifetime in 3C-SiC plotted against doping values for both electrons and holes.

The doping dependence of the SRH lifetimes is modelled with the Scharfetter relation shown in (21). In Fig. 15 the SRH lifetimes are plotted for both carrier types in 3C-SiC. Carrier lifetimes vary in literature for 3C-SiC with the best reported measured values of 10-15μs [71]. Additionally, authors in [72] claim lifetime values are equal to 0.5μs, though without specifying the corresponding doping concentration. These values are strongly dependent on the quality of each unique heteroepitaxially grown material layer and are expected to lower due to electrically active traps. In this work, the values of 2.5μs for electrons and 0.5μs for holes are assumed. This is considered a reasonable assumption for SiC technology. The arbitrary reference doping concentration (N_{ref}) operates as a normalization constant. The parameter values for the Scharfetter model, as discussed, are presented in Table XI. Detailed lifetime maps and the inclusion of deep levels when modelling devices is expected to have a great impact on the lifetimes. Therefore, the model presented here assumes excellent crystal quality with small density of electrically active defects.

2.7. Auger recombination

The Auger mechanism is used to describe the band-to-band non-radiative recombination, a process that includes the emission of a phonon. The Auger recombination rate is described in (22) with temperature and doping dependence coefficients. These coefficients decrease when high injection conditions occur in the material as a consequence of the excitons decay [73]. Assuming room temperature, the Auger coefficients dependence on doping is expressed with the parameter $H_{n,p}$. In Fig. 16 this non-linear dependence is plotted for a range of carrier density values of $1.8 \times 10^{19} < N_D < 2.3 \times 10^{20}\text{cm}^{-3}$. Each carrier density value corresponds to a certain excitation energy. For highly doped n-regions, it can be assumed that $N_D \gg N_A$, thus the excess minority holes injection is negligible. Further, we assume a constant low value of excited holes p for the aforementioned range of excess carrier densities n when using (22). In order to be consistent with real material conditions, the effective intrinsic carrier concentration, $n_{i,eff}$, is calculated after taking into account the bandgap narrowing ($E_{g,eff}$) for the investigated doping levels as expressed in (1). Similarly, the exactly opposite can be considered for an excited highly doped p-type region, where $N_D \ll N_A$.

$$R_{net}^{A} = (C_n n + C_p p)(np - n_{i,eff}^2) \tag{22}$$

$$C_n(T,n) = \left(A_n + B_n\left(\frac{T}{T_0}\right) + C_n\left(\frac{T}{T_0}\right)^2\right)\left[1 + H_n exp\left(-\frac{n}{N0,n}\right)\right] \quad (23)$$

$$C_p(T,p) = \left(A_p + B_p\left(\frac{T}{T_0}\right) + C_p\left(\frac{T}{T_0}\right)^2\right)\left[1 + H_p exp\left(-\frac{p}{N0,p}\right)\right] \quad (24)$$

According to [74], it is safe to assume that in 3C-SiC the temperature dependence of Auger recombination coefficient is negligible. Hence, the parameter values presented in Table XII, are adopted. Essentially, in (23) and (24) the temperature parameters B_n and C_n are considered zero due to the lack of corresponding measurements. However, it is suggested that a related experimental work on 3C-SiC samples would be valuable and may provide better insight for the understanding of this mechanism.

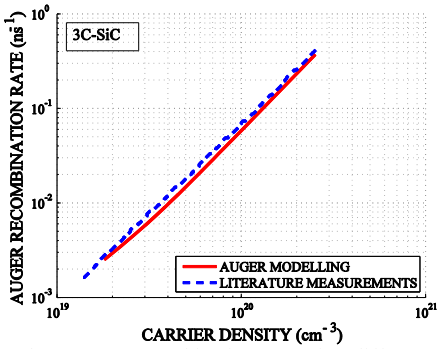

Fig. 16: The Auger recombination rate for different net doping concentration values, in an n-type 3C-SiC material. The independent variable values in the x-axis correspond to specific excitation levels in order to have a valid comparison with the measurements in [74].

Table XII: *3C-SiC Auger recombination rates.*

Parameter	***3C-SiC***	
	Electrons	Holes
coefficient A [cm⁶/sec]	$0.3x10^{-31}$	$0.2x10^{-31}$
coefficient B [cm⁶/sec]	0	0
coefficient C [cm⁶/sec]	0	0
coefficient H	1.9	1.9
N_0 [cm⁻³]	$1.0x10^{19}$	$1.0x10^{19}$
T_0 [K]	300	300

2.8. Thermal Conductivity of 3C-SiC

The thermal conductivity (κ) represents the rate of heat flow through a material. For SiC single crystal, values as high as 5 W/cmK are reported [75] [76]. However, most SiC devices are characterized by much smaller κ values. For the 3C-SiC, the majority of experimental works determine its thermal conductivity at 3.2 W/cmK, further for the 4H-SiC at the value of 3.7 W/cmK [40] [72] [77].

The resistivity model [76] shown in (25) can be used to indicate indirectly the thermal conductivity of the material by $\kappa = 1/\chi$ with a valid range of 200K - 600K. The parameters that give the best matching for 3C-SiC are presented in Table XIII. Fig. 17 summarizes the content of this subsection.

$$\chi = (1/kappa) + (1/kappa\_b)T + (1/kappa\_c)T^2 \quad (25)$$

Table XIII: Thermal Resistivity parameter values for the 3C-SiC

Parameters Description	***3C-SiC***
1/kappa [K·cm/W]	$4.4x10^{-2}$
1/kappa_b [cm/W]	$4.0x10^{-4}$
1/kappa_c [cm/K·W]	$1.65x10^{-6}$

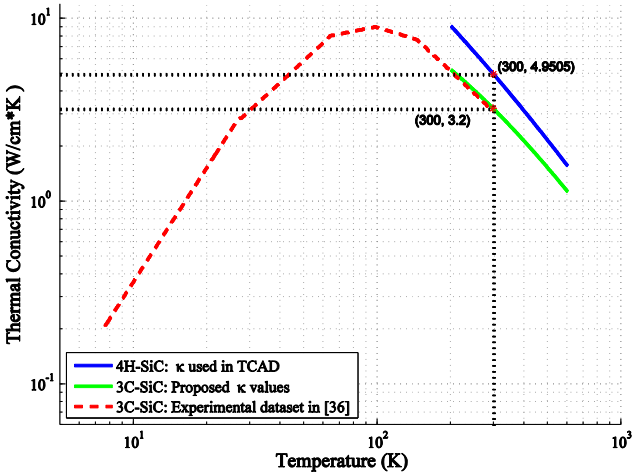

Fig. 17: The thermal resistivity parameters determined in this sub-section are in excellent agreement to the literature data. This work implies that what was assumed until now for both the 3C-SiC and the 4H-SiC was not a good approximation.

3. Conclusions

This work introduced for the first time a comprehensive set of models and their parameter values for bulk 3C-SiC. For each property of the semiconductor material, an appropriate model was suggested and the model parameter values were defined. The selected models and parameters were validated against published experimental data from studies that aimed to characterize aspects of the performance of 3C-SiC. The extensive review of the literature revealed that, compared to other materials, for example the 4H-SiC or Silicon, there was less published data available. Nonetheless, sufficient data was collated to model the bandgap and electron affinity, the density of states, carriers' mobility at low and high field, impact ionization, incomplete ionization, recombination phenomena and thermal conductivity. Special attention was given in accurately modelling the temperature dependence and the dependence on doping of these properties. For most properties and physical phenomena, the models proposed with the parameters could accurately predict the performance of the material and match the experimental data for a large range of temperatures. The validation process also highlighted that for some cases, the behavior could only be replicated for a limited range of temperatures. For these, good matching was achieved for the range of temperatures where devices are typically designed for or analyzed for, that is for $300\text{K} < T < 500\text{K}$. For research focusing on the physical properties outside of this region, new expressions will need to be developed. This work also aimed for the models selected and the parameters defined to be completely compatible and easily embeddable in TCAD software packages, for example the Synopsys Sentaurus Advanced TCAD. The use of credible models in this context allows for trustworthy device design optimization with bulk 3C-SiC as the material of choice.

References

[1] H. a. Toliyat, "Recent advances and applications of power electronics and Motor Drives - Electric machines and motor drives," *2008 34th Annu. Conf. IEEE Ind. Electron.*, 2008.

[2] J. Millan, P. Godignon, X. Perpina, A. Perez-Tomas, and J. Rebollo, "A Survey of Wide Bandgap Power Semiconductor Devices," *IEEE Trans. Power Electron.*, vol. 29, no. 5, pp. 2155–2163, 2014.

[3] N. G. Wright, A. B. Horsfall, and K. Vassilevski, "Prospects for SiC electronics and sensors," *Mater. Today*, vol. 11, no. 1–2, pp. 16–21, 2008.

[4] A. R. Powell and L. B. Rowland, "SiC materials-progress, status, and potential roadblocks," *Proc. IEEE*, vol. 90, no. 6, pp. 942–955, 2002.

[5] H. Morkoç, S. Strite, G. B. Gao, M. E. Lin, B. Sverdlov, and M. Burns, "Large-band-gap SiC, III-V nitride, and II-VI ZnSe-based semiconductor device technologies," *J. Appl. Phys.*, vol. 76, no. 3, pp. 1363–1398, 1994.

[6] G. Ferro, "3C-SiC Heteroepitaxial Growth on Silicon: The Quest for Holy Grail," *Crit. Rev. Solid State Mater. Sci.*, vol. 40, no. 1, pp. 56–76, 2015.

[7] F. Ciobanu *et al.*, "Traps at the Interface of 3C-SiC/SiO₂-MOS-Structures," *Mater. Sci. Forum*, vol. 433–436, pp. 551–554, 2003.

[8] K. K. Lee, G. Pensl, M. Soueidan, G. Ferro, and Y. Monteil, "Very Low Interface State Density From Thermally Oxidized Single-Domain 3C–SiC/6H–SiC Grown by Vapour–Liquid–Solid Mechanism," *Jpn. J. Appl. Phys.*, vol. 45, 2006.

[9] J. Lorenzzi, R. Esteve, N. Jegenyes, S. A. Reshanov, A. Schöner, and G. Ferro, "3C-SiC MOS Based Devices: From Material Growth to Device Characterization," *Mater. Sci. Forum*, vol. 679–680, pp. 433–436, Mar. 2011.

[10] A. Schöner, M. Bakowski, P. Ericsson, H. Strömberg, H. Nagasawa, and M. Abe, "Realisation of Large Area 3C-SiC MOSFETs," *Mater. Sci. Forum*, vol. 483–485, pp. 801–804, 2005.

[11] K. M. Speer, P. G. Neudeck, D. J. Spry, A. J. Trunek, and P. Pirouz, "Cross-sectional TEM and KOH-Etch Studies of Extended Defects in 3C-SiC p + n Junction Diodes Grown on 4H-SiC Mesas," *J. Electron. Mater.*, vol. 37, no. 5, pp. 672–680, 2008.

[12] K. Nakayama *et al.*, "Behavior of Stacking Faults in TEDREC Phenomena for 4.5 kV SiCGT," *Mater. Sci. Forum*, vol. 600–603, pp. 1175–1178, 2009.

[13] K. Furukawa, A. Uemoto, Y. Fujii, M. Shigeta, A. Suzuki, and S. Nakajima, "Selective Growth and Schottky Diode Characteristics of β-SiC Single Crystal Films on Si (111) Substrates by Chemical Vapor Deposition," Extended Abstracts of the 19th Conference on Solid State Devices and Materials, Tokyo, pp. 231–234, 1987.

[14] P. Shenoy, a. Moki, B. J. Baliga, D. Alok, K. Wongchotigul, and M. Spencer, "Vertical Schottky barrier diodes on 3C-SiC grown on Si," *Proc. 1994 IEEE Int. Electron Devices Meet.*, pp. 411-414, 1994.

[15] K. Furukawa, A. Uemoto, M. Shigeta, A. Suzuki, and S. Nakajima, "3C-SiC p-n junction diodes," *Appl. Phys. Lett.*, vol. 48, pp. 1536–1537, 1986.

[16] P. G. Neudeck, D. J. Larkin, J. E. Starr, J. a. Powell, C. S. Salupo, and L. G. Matus, "Greatly improved 3C-SiC p-n junction diodes grown by chemical vapor deposition," *IEEE Electron Device Lett.*, vol. 14, no. 3, pp. 136–139, 1993.
[17] M. Bakowski, A. Schöner, P. Ericsson, H. Strömberg, H. Nagasawa, and A. Masayuki, "Development of 3C-SiC MOSFETs," *J. Telecommun. Inf. Technol.*, pp. 49–56, 2007.
[18] Y. Watanabe, N. Kawana, T. Horikawa, and K. Kamimura, "Electrical Characterization of 3C-SiC Lateral MOSFETs Fabricated on Heteroepitaxial Films Including High Density of Defects," *Mater. Sci. Forum*, vol. 821–823, pp. 733–736, Jun. 2015.
[19] M. Kato, K. Miyake, T. Yasuda, M. Ichimura, T. Hatayama, and T. Ohshima, "Spectral response, carrier lifetime, and photocurrents of SiC photocathodes," *Jpn. J. Appl. Phys.*, vol. 55, 2015.
[20] Y. Fu, L. Zhanming, N. Wai Tung, and S. J. Kin On, *Integrated Power Devices and TCAD Simulatons*. CRC Press, 2014.
[21] K. Hamada, "Challenge of adopting TCAD in the development of power semiconductor devices for automotive applications," *Int. Conf. Simul. Semicond. Process. Devices, SISPAD*, pp. 9–12, 2014.
[22] P. D. Lungu, "Modelling of SiC vertical power DMOSFET structure using the fundamental MOSFET's set of equations," *Int. Semicond. Conf.*, vol. 2, no. 3, pp. 27–30, 1996.
[23] K. F. Brennan *et al.*, "Materials theory based modeling of wide band gap semiconductors: from basic properties to devices," *Solid. State. Electron.*, vol. 44, no. 2, pp. 195–204, Feb. 2000.
[24] Z. Rong, F. Gao, and W. J. Weber, "Monte Carlo simulations of defect recovery within a 10 keV collision cascade in 3C–SiC," *J. Appl. Phys.*, vol. 102, 2007.
[25] A. Arvanitopoulos, S. Perkins, K. N. Gyftakis, M. Antoniou, and N. Lophitis, "3C-SiC material parameters for accurate TCAD modeling and simulation," in 10th *ICSI*, Warwick, 2017.
[26] F. Li, Y. Sharma, M. Jennings, H. Rong, C. Fisher, and P. Mawby, "Study of a novel lateral RESURF 3C-SiC on Si Schottky diode," *2014 16th Eur. Conf. Power Electron. Appl. EPE-ECCE Eur. 2014*, pp. 1–10, 2014.
[27] F. Li, Y. K. Sharma, C. A. Fisher, M. R. Jennings, and P. A. Mawby, "A novel 3C-SiC on Si power Schottky diode design and modelling," *MRS Proc.*, vol. 1693, no. January, p. mrss14-1693-dd06-16, 2014.
[28] A. Arvanitopoulos, N. Lophitis, K. N. Gyftakis, M. Belanche Guadas, S. Perkins, and M. Antoniou, "Physical parameterisation of 3C- Silicon Carbide (SiC) with scope to evaluate the suitability of the material for power diodes as an alternative to 4H- SiC," in *IEEE SDEMPED*, 2017.
[29] A. Qamar, P. Tanner, D. V. Dao, H. Phan, and T. Dinh, "Electrical Properties of p-type 3C-SiC / Si Heterojunction Diode Under Mechanical Stress," vol. 35, no. 12, pp. 1293–1295, 2014.
[30] G. Colston and M. Myronov, "Effect of Thickness on the Optical Properties of monocrystalline 3C-SiC Epilayers grown on Silicon," in 10th *ICSI*, Warwick, 2017.
[31] W. Bludau and A. Onton, "Temperature dependence of the band gap of silicon," *J. Appl. Phys.*, vol. 45, no. 4, 1974.
[32] K. Rogdakis *et al.*, "Theoretical comparison of 3C-SiC and Si nanowire FETs in ballistic and diffusive regimes," *Nanotechnology*, vol. 18, no. 47, p. 475715, 2007.
[33] W. J. Choyke and L. Patrick, "Optical properties of polytypes of SiC: interband absorption, and luminescence of nitrogen-exciton complexes.," *Mater. Res. Bull*, vol. 4, p. 141, 1969.
[34] U. Lindefelt, "Doping-induced band edge displacements and band gap narrowing in 3C–, 4H–, 6H–SiC, and Si," *J. Appl. Phys.*, vol. 84, no. 5, pp. 2628–2637, 1998.
[35] S. C. Jain and D. J. Roulston, "A simple expression for band gap narrowing (BGN) in heavily doped Si, Ge, GaAs and GexSi1−x strained layers," *Solid. State. Electron.*, vol. 34, no. 5, pp. 453–465, May 1991.
[36] "Silicon Carbide." [Online]. Available: http://www.ioffe.ru/SVA/NSM/Semicond/SiC. [Accessed: 01-Jan-2017].
[37] S. Y. Davydov, "On the electron affinity of silicon carbide polytypes," *Semiconductors*, vol. 41, no. 6, pp. 696–698, 2007.
[38] L. Patrick and W. J. Choyke, "Static dielectric constant of SiC," *Phys. Rev. B*, vol. 2, no. 6, pp. 2255–2256, 1970.
[39] M. Ruff, H. Mitlehner, and R. Helbig, "SiC devices: Physics and numerical simulation," *IEEE Trans. Electron Devices*, vol. 41, no. 6, pp. 1040–1054, 1994.
[40] J. B. Casady and R. W. Johnson, "Status of silicon carbide (SiC) as a wide-bandgap semiconductor for high-temperature applications: A review," *Solid. State. Electron.*, vol. 39, no. 10, pp. 1409–1422, 1996.
[41] R. F. Pierret, *Semiconductor Device Fundamentals*. Addison-Wesley Publishing Co., 1996.
[42] Y. Goldberg, M. Levinshtein, and S. Rumyantsev, "Silicon Carbide (SiC)," in *Properties of advanced semiconductor materials : GaN, AlN, InN, BN, SiC, SiGe*, M. E. Levinshtein, S. L. Rumyantsev, and M. S. Shur, Eds. New York: Wiley, 2001.
[43] N. D. Arora, J. R. Hauser, and D. J. Roulston, "Electron and Hole Mobilities in Silicon as a Function of Concentration and Temperature," *IEEE Trans. Electron Devices*, vol. 29, no. 2, pp. 292–295, 1982.
[44] D. M. Caughey and R. E. Thomas, "Carrier Mobilities in Silicon Empirically Related to Doping and Field," *Proc. IEEE*, vol. 55, no. 12, pp. 2192–2193, 1967.
[45] M. Roschke and F. Schwierz, "Electron mobility models for 4H, 6H, and 3C SiC," *IEEE Trans. Electron Devices*, vol. 48, no. 7, pp. 1442–1447, 2001.
[46] J. A. Powell, L. G. Matus, and M. A. Kuczmarski, "Growth and Characterization of Cubic SiC Single-Crystal Films on Si," *J. Electrochem. Soc. Solid State Sci. Technol.*, vol. 134, pp. 1558–1565, 1987.
[47] Y. Chen, X. Zhang, Q. Zhao, L. He, C. Huang, and Z. Xie, "P-type 3C-SiC nanowires and their optical and electrical transport properties," *Chem. Commun.*, vol. 47, no. 22, p. 6398, 2011.

[48] E. Bellotti, H. E. Nilsson, K. F. Brennan, P. P. Ruden, and R. Trew, "Ensemble Monte Carlo calculation of hole transport in bulk 3C–SiC," *J. Appl. Phys.*, vol. 87, 2000.
[49] N. Piluso, A. Severino, M. Camarda, A. Canino, A. La Magna, and F. La Via, "Raman study of bulk mobility in 3C-SiC heteroepitaxy," *Mater. Sci. Forum*, vol. 679–680, pp. 221–224, 2011.
[50] H. Matsuura, Y. Masuda, Y. Chen, and S. Nishino, "Determination of donor densities and donor levels in 3C-SiC grown from Si2(CH3)6 using Hall-effect measurements," *Japanese J. Appl. Physics, Part 1 Regul. Pap. Short Notes Rev. Pap.*, vol. 39, no. 9 A, pp. 5069–5075, 2000.
[51] T. Yeghoyan, K. Alassaad, V. Soulière, and G. Ferro, "Silicon Deposition on 3C-SiC Seeds of Different Orientations," *Mater. Sci. Forum*, vol. 897, no. 100, pp. 87–90, 2017.
[52] K. Shiojima, M. Shingo, N. Ichikawa, and M. Kato, "Two-dimensional characterization of 3C-SiC layers using scanning internal photoemission microscopy : Mapping of electrical characteristics and crystal quality in domain boundary regions Two-dimensional characterization of 3C-SiC layers using scanning inte," *Jpn. J. Appl. Phys.*, vol. 56, no. 4S, pp. 3–7, 2017.
[53] M. Myronov and C. Morrison, "2D holes mobility anisotropy in strained epitaxial Germanium," in 10th *ICSI*, Warwick, 2017.
[54] C. M. Zetterling *et al.*, "Bipolar integrated circuits in SiC for extreme environment operation," *Semicond. Sci. Technol.*, vol. 32, no. 3, 2017.
[55] C. Canali, G. Majni, R. Minder, and G. Ottaviani, "Electron and hole drift velocity measurements in silicon and their empirical relation to electric field and temperature," *IEEE Trans. Electron Devices*, vol. 22, no. 11, pp. 1045–1047, 1975.
[56] B. J. Baliga, *Fundamentals of Power Semiconductor Devices*. New York: Springer, 2008.
[57] C. Codreanu, M. Avram, E. Carbunescu, and E. Iliescu, "Comparison of 3C–SiC, 6H–SiC and 4H–SiC MESFETs performances," *Mater. Sci. Semicond. Process.*, vol. 3, pp. 137–142, 2000.
[58] R. P. Joshi and D. K. Ferry, "Calculations of the temperature and field dependent electronic mobility in β-SiC," *Solid. State. Electron.*, vol. 38, no. 11, pp. 1911–1916, 1995.
[59] L. Tirino, M. Weber, K. F. Brennan, E. Bellotti, and M. Goano, "Temperature dependence of the impact ionization coefficients in GaAs, cubic SiC, and zinc-blende GaN," *J. Appl. Phys.*, vol. 94, no. 1, pp. 423–430, 2003.
[60] A. G. Chynoweth, "Ionization Rates for Electrons and Holes in Silicon," *Phys. Rev.*, vol. 109, no. 5, pp. 1537–1540, 1957.
[61] R. Van Overstraeten and H. De Man, "Measurement of the ionization rates in diffused silicon p-n junctions," *Solid State Electron.*, vol. 13, no. 5, pp. 583–608, 1970.
[62] C. Raynaud, D. Tournier, H. Morel, and D. Planson, "Comparison of high voltage and high temperature performances of wide bandgap semiconductors for vertical power devices," *Diam. Relat. Mater.*, vol. 19, no. 1, pp. 1–6, 2010.
[63] F. C. Beyer, "Deep Levels in SiC," Chemistry and Biology Linkoping University, 2011.
[64] a. a. Lebedev, "Deep level centers in silicon carbide: A review," *Semiconductors*, vol. 33, no. 2, pp. 107–130, 1999.
[65] H. Kuwabara, S. Yamada, and S. Tsunekawa, "Radiative recombination in β-SiC doped with boron," *J. Lumin.*, vol. 12–13, pp. 531–536, Mar. 1976.
[66] H. Kuwabara and S. Yamada, "Free-to-bound transition in β-SiC doped with boron," *Phys. Status Solidi Appl. Mater. Sci.*, vol. 30, no. 2, pp. 739–746, 1975.
[67] H. Kuwabara, K. Yamanaka, and S. Yamada, "Donor-acceptor pair emission from β-sic doped with gallium," *Phys. Status Solidi Appl. Mater. Sci.*, vol. 37, no. 2, pp. 157–161, 1976.
[68] K. F. Dombrowski, U. Kaufmann, M. Kunzer, K. Maier, and J. Schneider, "Deep donor state of vanadium in cubic silicon carbide (3C-SiC)," *Appl. Phys. Lett.*, vol. 65, pp. 1811–1813, 1994.
[69] A. V. Bolotnikov, P. G. Muzykov, A. E. Grekov, and T. S. Sudarshan, "Improvement of 4H-SiC power p-i-n diode switching performance through local lifetime control using boron diffusion," *IEEE Trans. Electron Devices*, vol. 54, no. 6, pp. 1540–1544, 2007.
[70] G. L. Harris, *Properties of silicon carbide*. London: EMIS Datareviews Series No.13, 1995.
[71] J. Sun *et al.*, "Considerably long carrier lifetimes in high- quality 3C-SiC (111)," *Appl. Phys. Lett.*, vol. 25, 2012.
[72] A. Aditya, S. Khandelwal, C. Mukherjee, A. Khan, S. Panda, and B. Maji, "Search of appropriate semiconductor for PIN Diode fabrication in terms of resistance analysis," *2015 Int. Conf. Recent Dev. Control. Autom. Power Eng. RDCAPE 2015*, pp. 61–65, 2015.
[73] R. Häcker and A. Hangleiter, "Intrinsic upper limits of the carrier lifetime in silicon," *J. Appl. Phys.*, vol. 75, no. 11, 1994.
[74] P. Ščajev, V. Gudelis, K. Jarašiūnas, and P. B. Klein, "Fast and slow carrier recombination transients in highly excited 4H- and 3C-SiC crystals at room temperature," *J. Appl. Phys.*, vol. 108, no. 2, 2010.
[75] R. Yakimova, R. Vasiliauskas, J. Eriksson, and M. Syväjärvi, "Progress in 3C-SiC Growth and Novel Applications," *Mater. Sci. Forum*, vol. 7, no. 11, pp. 3–10, 2012.
[76] M. Lades, "Modeling and Simulation of Wide Bandgap Semiconductor Devices : 4H / 6H-SiC," in Selected Topics of Electronics and Micromechatronics Aachen: Shaker Verlag, vol. 3, Technical University of Munchen, 2002.
[77] G. Rosario and R. Gerhardt, *Properties and applications of silicon carbide*. InTech, 2011.